Journal of the Korean Chemical Society
2023, *Vol. 67, No. 3*
Printed in the Republic of Korea
https://doi.org/10.5012/jkcs.2023.67.3.175

Synthesis and Band Gap Analysis of *Meso*-Arylporphyrins Containing Exclusively Electron Donating or Withdrawing Groups

Min Su Kang and Kwang-Jin Hwang*
Department of Bio & Chemical Engineering, Hongik University, Sejong 339-701, Korea.
**E-mail: kjhwang@hongik.ac.kr*
(Received March 15, 2023; Accepted April 25, 2023)

ABSTRACT. *Tetra*-aryl substituted A4-type porphyrins (**TP**, **TD**, **TA**) and *trans*-A2B2 porphyrins (**DDP1**, **AAP1**) with electron-donating or withdrawing groups were synthesized. The band gap energy of those porphyrins was calculated from their UV-Vis spectra and CV data. With an electron-withdrawing group, the band gap energy of porphyrin **TA** increased via the LUMO energy up. Meanwhile, the introduction of an electron-donating group decreased the band gap of porphyrin by HOMO level up as as in the case of porphyrin **TD**. The band gap (2.19-2.28 eV) of metalloporphyrin **PP-Ni** was greater than those (1.81-2.06 eV) of non-metalloporphyrins **PP** due to the LUMO level up.

Key words: Porphyrin, Metalloporphyrin, Band gap, HOMO, LUMO

INTRODUCTION

The band gap energy (E_g) of organic materials is the energy difference between the HOMO and the LUMO energy of those. The band gap is known to be one of the important properties for application in the organic light-emitting device (OLED) and organic photovoltaic (OPV) devices.[1,2] Depending on the band gap of organic electronic materials, the emission or absorption wavelength, charge injection or transfer, and the device's efficiency could be adjusted. To obtain a long-wavelength absorption in photovoltaics and electroluminescence, the structural modification of copolymers as well as counter monomers are processed leading to low band gap energy.[2-4]

Porphyrin has been applied as a sensitizer in P3HT [poly(3-hexylthiophene)]-PCBM(phenyl-C61-butyric acid methyl ester) based organic heterojunction solar cells in a role of a light-harvesting with a high extinction coefficient at an adequate wavelength.[5-7] To avoid overlap with the absorption by the donor, a proper band gap (HOMO and LUMO energy level) of porphyrins is required for efficient electron and hole transfer between the donor and acceptor. The band gap of porphyrins has been known to be dependent on the variation of substituent, incorporating metal, length of the conjugation, and working environment.[3,8]

Previously, we have reported the substituent effect on the band gap of porphyrin (**PP**) derivatives.[8] In a continuation effort, we designed meso-tetraarylporphyrins (**TP**, **TD**, and **TA**) in which only electron-donating (EDG) or accepting (EWG) groups are attached to the aryl groups as in *Fig.* 1. Here, we report the synthesis of tetra-aryl A4-porphyrins (**TP1**, **TP2**, **TD**, **TA**) and A2B2 porphyrin (**DDP1**, **AAP1**) derivatives with metalloporphyrin (**PP-Ni**) and their band gap with the HOMO-LUMO energy analyzed from the electro and spectroscopic data.

On Occasion of the retirement of Professor Hwang from Hongik University at Sejong in August of 2023.

EXPERIMENTAL

General Information

All reactions were carried out under atmospheric dry N_2 pressure. The solvent $CHCl_3$ was dried by distillation with P_2O_5. For solution-state NMR data, JNM-LAMDA (300 MHz) was used with $CDCl_3$ as solvent and Mass data were collected from JMS-700 (Jeol) for FAB ionization at the Korea Research Institute of Chemical Technology. UV-Visible and emission spectroscopy were collected on Evolution 60S (Thermo Scientific) and Cary eclipse fluorescence spectrophotometer (Varian) respectively. Cyclic voltammetry was measured on a Versa STAT3 (AMETEK) at Korea University (Sejong). A three-electrode system was used and consisted of a reference electrode (Ag/AgCl), a working electrode (sample-coated TiO_2 films and Pt plate), and a counter electrode (Pt wire). The redox potentials of porphyrins were measured in tetrahydrofuran with 0.1M $TBAPF_6$ with a scan rate of 50 mV s^{-1}.

For the organic synthesis of all porphyrin derivatives,

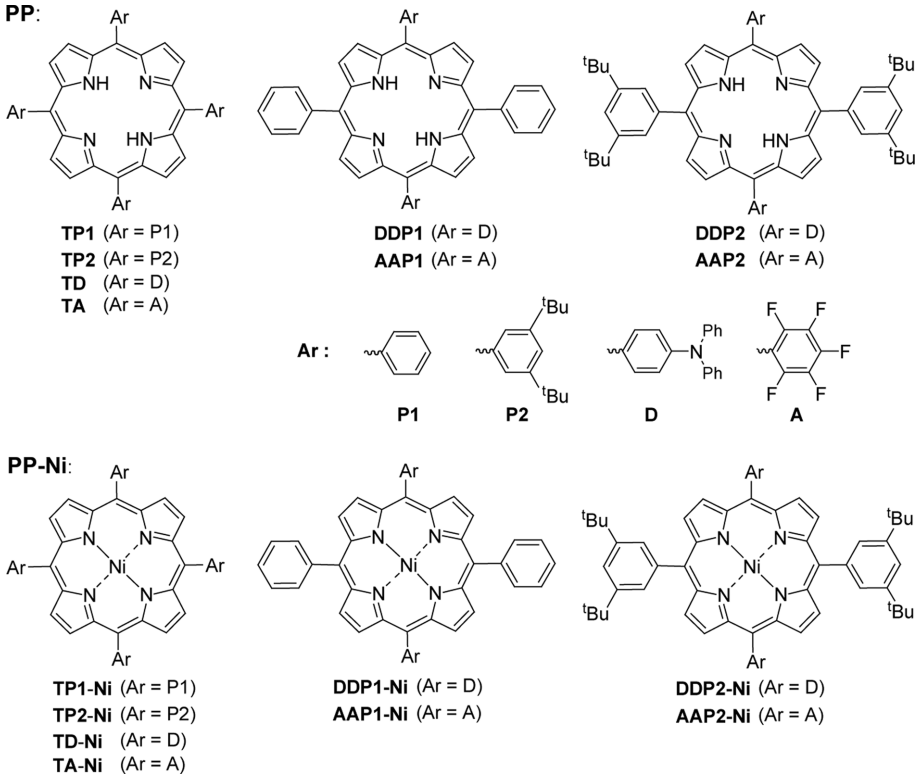

***Figure* 1.** Chemical structures of *tetra*-arylporphyrin (PP) and *nickel*-contained porphyrin (PP-Ni) derivatives.

similar procedures in literature[8] were applied with minor modifications unless specified. All the structure identification was confirmed using NMR (300 MHz, $CDCl_3$) and FAB Mass spectroscopic data.

2,2′-((Phenyl)methylene)bis(1H-pyrrole) (2P1). Yield; 95%, yellow solid: ^{1}H NMR δ (ppm) 7.87 (s, 2H, NH), 7.13-7.27 (m, 5H, ArH), 6.62-6.64 (dd, J = 3 Hz, 3 Hz, 2H, α-pyrrole), 6.07-6.10 (dd, J = 3 Hz, 3 Hz, 2H, β-pyrrole), 5.85 (s, 2H, β-pyrrole), 5.41 (s, 2H, CH).

2,2′-((3,5-Di-*tert*-phenyl)methylene)bis(1H-pyrrole) (2P2). Yield; 73%, brown solid: ^{1}H NMR δ (ppm) 7.91 (s, 2H, NH), 7.31 (s, 1H, *p*-ArH), 7.05-7.06 (d, J = 3 Hz, 2H, *o*-ArH), 6.67-6.68 (d, J = 3 Hz, 2H, α-pyrrole), 6.13-6.16 (dd, J = 3 Hz, 3 Hz, 2H, β-pyrrole), 5.93 (s, 2H, β-pyrrole), 5.44 (s, 1H, CH), 1.25-1.28 (d, J = 9 Hz, 18H, CH_3).

5,10,15,20-Tetrakis(phenyl)porphyrin (TP1). To the solution of bispyrrole, **2P1** (0.33 g, 1.5 mmol) and benzaldehyde (0.16 g, 1.5 mmol) in $CHCl_3$ (10 ml) was added $BF_3{\cdot}OEt_2$ (0.20 ml of 2.5 M solution in $CHCl_3$, 0.49 mmol) at room temperature. After being stirred for 1 h, 2,3-dichloro-5,6-dicyano-*p*-benzoquinone (DDQ) (0.51 g, 2.25 mmol) was added and stirred for 1h more. The solution was evaporated, then added CH_2Cl_2 and 0.1N aqueous NaOH solution. The organic layer was dried with $MgSO_4$ and then evaporated. Isolation using column chromatography (SiO_2, 10% CH_2Cl_2 in *n*-hexane) gave purple solid **TP1**(65%): ^{1}H NMR d (ppm) 8.77 (s, 8H, β-pyrrole), 8.13 - 8.15 (d, J = 6 Hz, 8H, *o*-ArH-PP), 7.65-7.69 (dd, J = 6 Hz, 6 Hz, 12H, *m,p*-ArH-PP), -2.85 (s, 2H, inner NH). MS (FAB) m/z; calcd exact mass for $C_{44}H_{30}N_4$ 614.75, obs 615.

5,10,15,20-Tetrakis(3,5-di-*tert*-butylphenyl)porphyrin (TP2). Yield; 62%, purple solid: ^{1}H NMR δ (ppm) 8.82 (s, *8*H, β-pyrrole), 8.01 (s, 8H, *o*-ArH-PP), 7.71 (s, 4H, *p*-ArH-PP), 1.44 (s, 72H, CH_3) -2.75 (s, 2H, inner NH). MS (FAB) m/z; calcd exact mass for $C_{76}H_{94}N_4$ 1063.62, obs 1063.

5,10,15,20-Tetrakis(4-(diphenylamino)phenyl)porphyrin (TD). Yield; 44%, purple solid: ^{1}H NMR δ (ppm) 8.98 (s, 8H, β-pyrrole), 8.31-8.34 (d, J = 9 Hz, 8H, PP-ArH-N), 8.06-8.08 (d, J = 9 Hz, 8H, PP-ArH-N), 7.40-7.46 (m, 40H, ArH-PP), -2.69 (s, 2H, inner NH). MS (FAB) m/z; calcd exact mass for $C_{92}H_{66}N_8$ 1283.60, obs 1284.

5,10,15,20-Tetrakis(pentafluorophenyl)porphyrin (TA). Yield; 47%, purple solid: ^{1}H NMR δ (ppm) 8.84 (s, 8H, β-pyrrole), -2.99 (s, 2H, inner NH). MS (FAB) m/z; calcd exact mass for $C_{44}H_{10}F_{20}N_4$ 974.56, obs 975.

5,15-Bis(4-(diphenylamino)phenyl)-10,20-bis(phenyl)-porphyrin (DDP1). Yield; 31%, purple solid: ^{1}H NMR δ

(ppm) 8.99-9.00 (m, 4H, *β*-pyrrole), 8.84 (m, 4H, *β*-pyrrole), 8.21 - 8.23 (m, 8H, *o*-C_6H_5-N), 8.06-8.09 (m, 4H, *o*-PhH-PP), 7.77 (m, 6H, *m,p*-PhH-PP), 7.52-7.55 (m, 4H, PP-ArH-N), 7.40-7.46 (m, 12H, *m*, *p*-C_6H_5-N), 7.14-7.15 (m, 4H, PP-ArH-N), 2.75 (s, 2H, inner NH). MS (FAB) m/z; calcd exact mass for $C_{68}H_{48}N_6$ 949.17, obs 950.

5,15-Bis(pentafluorophenyl)-10,20-bis(phenyl)porphyrin (AAP1). Yield; 67%, purple solid: ^{1}H NMR δ (ppm) 8.87- 8.89 (d, *J* = 6 Hz, 4H, *β*-pyrrole), 8.72-8.74 (d, *J* = 6 Hz, 4H, *β*-pyrrole), 8.13-8.16 (dd, *J* = 3 Hz, 3 Hz, 4H, *o*-ArH-PP), 7.69-7.76 (dd, *J* = 6 Hz, 6 Hz, 6H, *m*, *p*-ArH-PP), -2.91 (s, 2H, inner NH). MS (FAB) m/z; calcd exact mass for $C_{44}H_{20}F_{10}N_4$ 794.66, obs 795.

[5,10,15,20-Tetrakis(phenyl)porphyrin]nickel(II) complex (TP1-Ni). Yield; 56%, red solid: ^{1}H NMR δ (ppm) 8.74 (s, 8H, *β*-pyrrole), 8.22 (m, 8H, *o*-ArH-PP), 7.69 (s, 12H, *m,p*-ArH-PP). MS (FAB) m/z; calcd exact mass for $C_{44}H_{28}N_4Ni$ 671.43, obs 670.

[5,10,15,20-Tetrakis(3,5-di-*tert*-butylphenyl)porphyrin] nickel(II) complex (TP2-Ni). Yield; 52%, red solid: ^{1}H NMR δ (ppm) 8.73 (s, 8H, *β*-pyrrole), 7.80 (s, 8H, *o*-ArH-PP), 7.63 (s, 4H, *p*-ArH-PP), 1.39 (s, 72H, CH_3). MS (FAB) m/z; calcd exact mass for $C_{76}H_{92}N_4Ni$ 1120.29, obs 1120.

[5,10,15,20-Tetrakis(pentafluorophenyl)porphyrin] nickel(II) complex (TA-Ni). Yield; 37%, purple solid: ^{1}H-NMR δ (ppm) 8.81 (s, 8H, *β*-pyrrole). MS (FAB) m/z; calcd exact mass for $C_{44}H_8F_{20}N_4Ni$ 1031.24, obs 941(M-90).

[5,15-Bis(pentafluorophenyl)-10,20-bis(phenyl) porphyrin]nickel(II) complex (AAP1-Ni). Yield; 53%, red solid: ^{1}H NMR δ (ppm) 8.89 (s, 4H, *β*-pyrrole), 8.74 (s, 4H, *β*-pyrrole), 8.14 (m, 4H, *o*-ArH-PP), 7.70 (m, 6 Hz, 6H, *m*, *p*-ArH-PP). MS (FAB) m/z; calcd exact mass for $C_{44}H_{18}F_{10}N_4Ni$ 851.33, obs 852.

RESULTS AND DISCUSSION

Synthesis

As shown in *Scheme* 1, *tetra*-substituted A_4-type porphyrins (**TP1**, **TP2**, **TD**, **TA**) were synthesized by McDonald coupling of bispyrrole **2** with the corresponding benzaldehyde **1** as a key step with minor modification of the known procedures.[8,10,11] Bispyrrole **2** was prepared by condensation of the corresponding aryl aldehyde **1** with an excess amount of pyrrole using an $InCl_3$ catalyst over 70% yield. Coupling of bispyrrole **2** with benzaldehyde **1** proceeded under BF_3 in $CHCl_3$ and was followed by *in situ* DDQ oxidation to give reddish fluorescent A_4-porphyrin **TP1**, **TP2**, **TD** and **TA** as well as *trans*-A_2B_2 porphyrin derivatives in 30-60% yield. All porphyrin derivatives were confirmed using the NMR and mass spectroscopic data. Internal ring-proton in porphyrins was assigned by a peak that appeared at a negative chemical shift (near -2.8 ppm). Metalloporphyrins were prepared by reaction with $Ni(OAc)_2$ in the chloroform-DMF solvent in about 37-56% yield. The metalation was characterized by the disappearance of the negative NMR peak. Metalloporphyrin **TD-Ni**, however, could not be afforded for unidentified reasons.

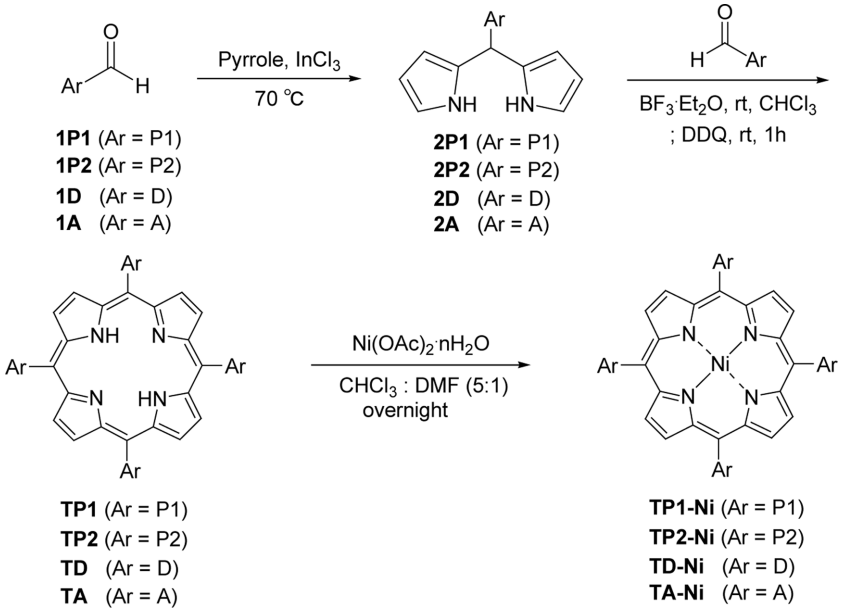

***Scheme* 1.** Synthetic route for meso-tetraaryl porphyrins.

Symmetric *trans*-A2B2 porphyrins (**DDP1**, **AAP1**) and their Ni-incorporates were also prepared similarly to the methods used in A4-porphyrin. The condensation followed by oxidation of bispyrrol **2D** and **2A** with benzaldehyde gave **DDP1** and **AAP1** in 31, 67% respectively. The incorporation of Ni cation proceeded by the reaction with $Ni(OAc)_2$ in chloroform-DMF to give metalloporphyrin **AAP1-Ni** in 53% yield. However, metalloporphyrin **DDP1-Ni** could not be prepared as in the case of **TD-Ni**.

Spectroscopic Analysis of Band Gap

The UV-Vis and emission spectra of the porphyrin derivatives (**PP**, **PP-Ni**) were measured at 3.3×10^{-5} M in $CHCl_3$ as listed in *Table* 1. The band gap energy (E_g) was calculated using Eq. (1); the results are also shown in *Table* 1.

$$E_g\ [\text{eV}] = h\times c/\ (\lambda_{onset}\times10^{-9})\times(1.6\times10^{-19}) = 1240/\lambda_{onset} \quad (1)$$

$h = 6.626\times10^{-34}$ J/s, $1\text{eV} = 1.6\times10^{-19}$ J

$c = 3.0\times10^{8}$ m/s

λ_{onset} = cut-off wavelength

To determine the HOMO-LUMO energy level of porphyrins **PP** and **PP-M**, the cyclic voltammetry (CV) of those was measured. THF solutions containing porphyrins were coated as a film on TiO_2 films and Pt plate, with Ag/AgCl as reference electrode and ferrocene was used for potential standard.[11] Appling Eqs. (2) and (3), E_{HOMO} and E_{LUMO} values were calculated[12] and results are shown in *Table* 1.

$$E_{HOMO}\ [\text{eV}] = -4.8 - [E_{onset} - E_{1/2}(ferrocene)] \quad (2)$$

$E_{1/2}(ferrocene) = 1/2(E_{pc} + E_{pa}) = 1/2(776 + 506) = 641(\text{mV})$

Epc, *Epa*: cathodic and anodic peak potential

$$E_g\ [\text{eV}] = E_{HOMO} - E_{LUMO} \quad (3)$$

In the absorption spectra of all porphyrin derivatives, a strong Soret-band was observed at 413-450 nm. Without EDG, EWG, the absorption of **PP** appeared near 430 nm as in the case of **TP1**, **TP2** (entry 1,2). With a substitution of EWG, the Soret-absorption of **TA** showed a blue shift (entry 4, 424 nm) from 450 nm of **TD** (entry 3**).** This result suggested that the band gap of **PP** increases with EWG and decreases with EDG. The incorporation of nickel resulted in a distinct blue-shifted Soret band (**PP-Ni**, 415-426 nm) from those of the corresponding **PP** with one main Q-band peak near 530 nm. The emission of **PP** derivatives appeared with two peaks at 650-732 nm. Meanwhile, no significant emission peak of **PP-Ni** was observed.

***Table* 1.** Absorption, emission, and CV analysis and the band gap energy of porphyrin derivatives **PP** and **PP-Ni**

Porphyrin		Absorption (λ_{abs}, nm)[a,b]		Emission	λ_{onset}[d]	E_g[e]	E_{oneset}[f]	E_{HOMO}[g]	E_{LUMO}[g]
entry	Abbr	Soret band	Q-band	(λ_{max}, nm)[c]	(nm)	(eV)	(mV)	(eV)	(eV)
1	**TP1**	429(1.50)	526(0.06), 561(0.03), 600(0.02), 656(0.01)	652, 717	669	1.85	988	-5.15	-3.29
2	**TP2**	432(1.84)	529(0.07), 565(0.04), 604(0.02), 658(0.02)	654, 720	675	1.84	1002	-5.18	-3.34
3	**TD**	450(0.16)	535(0.03), 576(0.03), 663(0.02), 669(0.02)	676, 732	680	1.81	685	-4.84	-3.04
4	**TA**	424(2.02)	518(0.16), 593(0.06), 645(0.01)	641, 710	602	2.06	1020	-5.18	-3.12
5	**DDP1**	429(0.76)	525(0.03), 560.5(0.01), 600(0.01), 657(0.01)	647, 717	671	1.85	1080	-5.24	-3.39
6	**AAP1**	426(1.35)	522(0.07), 554(0.02), 597(0.02), 651(0.01)	647, 713	664	1.87	1080	-5.24	-3.37
7	**DDP2**[h]	424(0.93)	523(0.07), 561(0.06), 593(0.04), 656(0.03)	661	676	1.83	962	-5.12	-3.29
8	**AAP2**[h]	418(1.49)	517(0.08), 546(0.04), 588(0.05), 645(0.02)	645	630	1.97	1168	-5.33	-3.36
9	**TP1-Ni**	415(0.35)	526(0.02)	(ns)[i]	543	2.28	1000	-5.16	-2.88
10	**TP2-Ni**	418(0.29)	526(0.02)	(ns)	547	2.27	1000	-5.16	-2.89
11	**TA-Ni**	415(0.40)	525(0.02)	(ns)	566	2.19	1071	-5.23	-3.04
12	**AAP1-Ni**	415(0.80)	511(0.02), 546(0.02)	(ns)	564	2.20	1071	-5.23	-3.03
13	**DDP2-Ni**[h]	426(0.46)	533(0.05)	(ns)	560	2.21	994	-5.15	-2.94
14	**AAP2-Ni**[h]	413(0.88)	529(0.06), 561(0.04)	(ns)	578	2.15	1258	-5.42	-3.27

[a]UV absorption was measured at 3.3×10^{-5} M in $CHCl_3$.

[b]The absorbance values are shown in parentheses.

[c]Emission was measured with excitation at 420 nm.

[d]The intersection of the tangent line of an absorption peak at the longest wavelength with the baseline of UV spectrum.

[e]From the equation 1 was calculated.

[f]The voltage at the oxidation begins in CV diagram.

[g]The HOMO-LUMO energy values are calculated from Eqs. (2) and (3).

[h]All data are from the reference [17], UV absorption was measured at 5×10^{-6} M in $CHCl_3$.

[i]No significant emission intensity was observed.

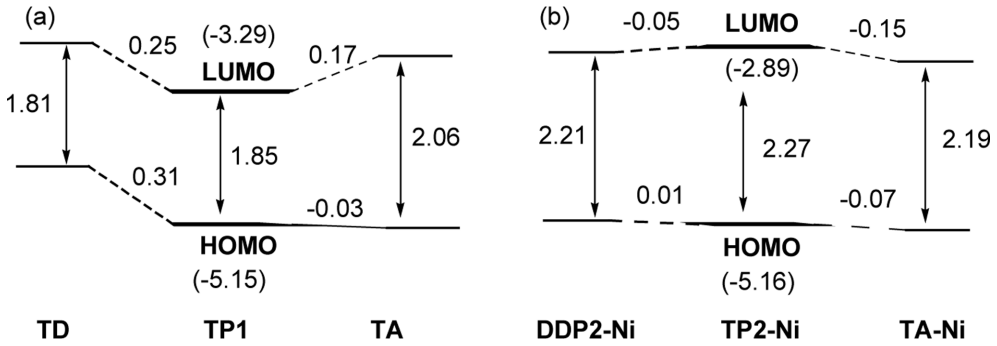

***Figure* 2.** The band gap (E_g) and HOMO-LUMO energy diagram of porphyrin **PP** (a) and **PP-Ni** (b) derivatives. E_g values are shown near the arrow and the numbers in parenthesis are MO's energy value in eV unit. The other numbers are the energy difference between the HOMOs or LUMOs of porphyrins in comparison.

As suggested from the UV-Vis spectroscopic data, the band gap (E_g) of **PP** derivatives depends on the substituent of its capacity of electron donation and withdrawal. For comparison, the energy diagram of representative **PP** and **PP-Ni** is represented in *Fig*. 2. With EWG, the band gap of tetra-aryl **PP** increased in the order of **TA** (2.06) > **TP1** (1.85) > **TD** (1.80). A similar result was also observed in A_2B_2 porphyrins (entry 5-8) such as **AAP1** (1.87) > **DDP1** (1.85). These results were considered to attribute that EWG in porphyrin **TA** induced an increase in LUMO energy (0.17 eV) with a decrease of HOMO energy (-0.03 eV) from those of **TP1** as presented in *Fig*. 2. Meanwhile, EDG in **TD** increased both HOMO (0.31 eV) and LUMO (0.25 eV) levels. Thus, the net result is a decreased band gap (1.81 eV) of **TD** from that of **TP1** (1.85 eV).

The substituent's electron push-pull tendency seems to affect HOMO and LUMO levels nonlinearly. This means a substituent effect on the up and down of HOMO and LUMO levels via inconsistent patterns. Thus, the band gap in porphyrin **PP** is the result of a net value of MO's energy. The more electron donation gave a smaller $\mathbf{E_{oneset}}$ (oxidation) value resulting in a higher HOMO energy level; **TD** (685 mV, -4.84 eV) < **TP1** (988 mV, -5.15 eV) < **TA** (1020 mV, -5.18 eV).

Metalation of **PP** elevated LUMO energy (-3.23 – -2.86) compared with the nonmetallic **PP** (-3.29 – -3.45). Thus, the band gap energy (-2.15 – -2.28 eV) of metalloporphyrin **PP-Ni** was greater than those of nonmetallic **PP** (1.80-2.06 eV). Both donor (entry 13) and acceptor (entry 11, 12, 14) groups in **PP-Ni** resulted in a decrease in the band gap from the **TP-Ni** (entry 9, 10). The substitution of EWG to **PP-Ni** lowered the LUMO level (-0.15) more than the HOMO energy (-0.07) to give decreased E_g (2.19 eV) of **TA-Ni** as in *Fig*. 2. Consequently, the acceptor group **A**($-C_6F_5$) mediated LUMO energy decrease was considered the most significant effect on the band gap in metalloporphyrin **PP-Ni**.

CONCLUSION

As a summary, we have synthesized A_4-porphyrin derivatives **TP1**, **TP2**, **TA** and **TD** and metalloporphyrins **PP-Ni**. The band gap with HOMO-LUMO levels of those **PP** and **PP-Ni** were analyzed from the UV-Vis and CV data. With EWG, the band gap of **PP** increased via the LUMO level up as the most remarkable effect. With an EDG, the band gap energy of **PP** decreased because of more HOMO energy up than the LUMO up. In the case of metalloporphyrin **TP-Ni**, the substitution of both EWG and EDG decreased the LUMO energy level and resulting in a reduced band gap from the tetraaryl porphyrins (**TP1**, **TP2)**.

Acknowledgments. This work was supported by academic research found at Hongik University (2022). The authors appreciate Professor Hwankyu Kim at Korea University (Sejong) for assistance to collect CV data.

REFERENCES

1. Sun, S.-S. *Organic and Polymeric Solar Cell* in Handbook of Organic Electronics and Photonics, Vol 3 Nalwa, H. S., Ed.; American Scientific Publisher: LA, USA, **2008**, Chap 7, p 313.
2. Perepichka, D. F.; Perepichka, I. F.; Meng, H.; Wudl, F. *Light-Emitting Polymers* in Organic Light-Emitting Materials and Device, Li, Z.; Meng, H., Eds.; CRC Press: Boca Raton, USA, **2007**, Chap 2, p 187.
3. Jones, D. *Flurene-Containing Polymers for Solar Cell Applications* in Organic Photovoltaics, Brabec, C.; Dyakonov, V.; Scherf, U., Eds.; Wiley-VCH Publisher: Weinheim, Germany, **2008**, Chap 2, p 76.
4. Ahn, S.-H.; Czae, M.-Z.; Kim, E.-R.; Lee, H.; Han, S.-H.;

Noh, J.; Hara, M. *Macromolecules*, **2001**, *34*, 2522.
5. a) Lyons, D. M.; Kesters, J.; Maes, W.; Bielawski, C. W.; Sessler, J. L. *Synth. Met.* **2013**, *178*, 56. b) Lash, T. D. *JPP* **2016**, *20*, 855.
6. Lee, J. Y.; Song, H. J.; Lee, S. M.; Lee, J. H.; Moon, D. K. *Eur. Polym. J.* **2011**, *47*, 1686.
7. a) Li, L.-L.; Diau, E. W.-G. *Chem. Soc. Rev.* **2013**, *42*, 291. b) El-Khouly, M. E.; Ito, O.; Smith, P. M.; D'Souza, F. *J. Photochem.* **2004**, *5*, 79.
8. Chang, I.-J.; Jeon, Y.-S.; Hwang, K.-J. *Bull. Korean Chem. Soc.* **2019**, *40*, 173.
9. Lee, J.-J.; Kim, Y. H.; Kang, S. K.; Choi, I. H.; Yi, J. H. *Kor. J. Chem. Eng.* **2006**, *23*, 512.
10. Cho, W.-S.; Kim, H.-J.; Littler, B. J.; Miller, M. A.; Lee, C.-H.; Lindsey, J. S. *J. Org. Chem.* **1999**, *64*, 7890.
11. Kang, S. H.; Jeong, M. J.; Eom, Y. K.; Choi, I. T.; Kwon, S. M.; Yoo, Y. J.; Kim, J. H.; Kwon, J.; Park, J. H.; Kim, H. K. *Adv. Energy Mater.* **2017**, *7*, 1602117.
12. Lee, H.; Kim, J. H. *Polymer Sci. Tech*. **2007**, *18*, 488.